INS/GNSS/Fiducial Marker Sensor Fusion for UAM Aircraft Navigation

Fábio Okina, Marcos R. O. A. Maximo, Marcelo Bruno and Daniel Viotti

Abstract—This paper addresses the sensor fusion of INS, GNSS, and Fiducial Markers for navigation in the Urban Air Mobility environment. The Error-State Kalman filter (ESKF) was adopted for the estimation of position, velocity, attitude, and biases, considering ideal and non-linear GNSS sensors in their tightly and loosely coupled forms. The main contribution of this work is the ESKF formulation for INS/GNSS/Fiducial Marker sensor fusion and validation with synthetic image simulation in the Unreal Engine integrated with Simulink. The Fiducial Marker fusion shows improvements in filter accuracy and corrects the filter when GNSS is not available.

Keywords—Sensor Fusion, INS, GNSS, Fiducial Marker

I. INTRODUCTION

Urban Air Mobility (UAM) aims to provide intra-urban transportation at a low cost. UAM vehicles will fly at low altitudes sharing airspace with other aircraft and may have pilots or be autonomously piloted [1].

Reliable and secure navigation is crucial for UAM vehicles and is challenging due to their operating conditions of low altitude and congested airspace [2].

The aircraft requirements and regulations for urban air mobility are topics of current research [4], [3]. Regarding navigation performance, the requirements point towards high precision and robust systems, leveraging information from onboard and ground sensors. To achieve the required navigation performance, sensor fusion techniques are suitable candidates for multi-sensor navigation systems.

INS/GNSS sensor fusion is one of the main approaches for improving navigation performance. The short-term accuracy and high frequency of the inertial sensors complement the global coverage and superior long-term error performance of the GNSS. By fusing these data one can improve the accuracy, availability, and robustness of the navigation [5], [6], [7].

Several filtering techniques have been developed for navigation sensor fusion. The classical approach is the Extended Kalman Filter (EKF) which provides a computationally efficient method for state estimation and has been subject to extensive research and application [8], [9].

Other approaches for INS/GNSS fusion are the Kalman Filter variations which do not depend on linearization such as the Sigma Point Kalman filter [10], [11] and the Unscented

Kalman Filter [9]. Particle filters are also an option for navigation sensor fusion [12].

The Error State (or Indirect) Kalman Filter (ESKF) [13] is an EKF variation which, instead of estimating the full state of the system, estimates only the errors. This approach has the advantage that the error states are better represented by linear dynamics than the full state. Furthermore, it also provides robustness in case of sensor failures, since INS integration is independent of correction sensors measurements. Comparative analysis shows that ESKF has better robustness to the imperfect tuning of the sensor noise covariance [14], [15] than the EKF.

In this paper, in addition to INS/GNSS we fuse fiducial markers for navigation aiding. Fiducial Markers such as April Tag [16], ArUco [17], ARToolKit [18], and ARTag [19] are features designed for automatic detection with monocular cameras, which can be applied for pose estimation and tracking [20], [21].

The main contributions of this work are as follows. The INS/GNSS/Fiducial Marker multi-sensor fusion solution for aircraft navigation with the ESKF, for estimation of position, velocity, attitude, and sensor biases. The validation of the filter in simulation with synthetic images in the Unreal Engine integrated with the Simulink environment. In this architecture the INS/GNSS fusion can provide accurate estimations and the Fiducial Marker can increase accuracy aiding the GNSS when in the field of view of the camera.

This paper is organized as follows. In Sec. II the equations of the Error State Kalman Filter are presented, in Sec. III the ESKF is formulated for navigation, in Sec. IV the update sensors are modelled, in Sec. V the simulation results and filter validation are shown. Finally in VI this paper is concluded.

II. THE ERROR STATE KALMAN FILTER

The Error State Kalman Filter is an EKF variation in which, instead of estimating the true states $x_{k,t}$ of the system, it follows an indirect approach where the nominal states x_k are integrated separately and only the error states δx_k are estimated by the filter. The relationship between true, nominal, and error states is

$$x_{k,t} = x_k + \delta x_k. \tag{1}$$

The system nominal states are integrated by

$$x_k = \int_0^{k\Delta t} f(x(t), u(t))dt. \tag{2}$$

where $f(\cdot)$ is a non linear function of the states x and inputs u. The prediction step estimates the error states δx

Fábio Okina, Aeronautical Engineering, Aeronautical Engineering, Aeronautics Institute of Technology (ITA) / EMBRAER, SJC-SP, e-mail: okina@ita.br; Marcos R. O. A. Máximo,Computer Science - Autonomous Computational Systems Lab (LAB-SCA), ITA, SJC-SP, e-mail: mmaximo@ita.br; Marcelo Bruno, Electronic Engineering, ITA, SJC-SP, e-mail: marcelo.bruno@gp.ita.br; Daniel Viotti, EMBRAER, SJC-SP, e-mail:daniel.viotti@embraer.com.br. This work was partially supported by ITA and EMBRAER. Marcos Maximo is partially funded by CNPq – National Research Council of Brazil through the grant (307525/2022-8).

and its covariance matrix P, with Jacobians of the error states evaluated at the nominal state

$$\widehat{\delta x}_{k|k-1} = F_x(x_k, u_k)\widehat{\delta x}_{k-1|k-1}, \qquad (3a)$$

$$P_{k|k-1} = F_x P_{k-1|k-1} F_x^T + F_i Q_i F_i^T. \qquad (3b)$$

where F_x is the Jacobian of f and Q_i is the covariance matrix of the perturbations. The update step corrects the error states when sensor measurements z_k are available:

$$K_k = P_{k|k-1}H_k^T(H_k P_{k|k-1}H_k^T + V)^{-1},$$
$$\widehat{\delta x}_{k|k}^- = K_k(z_k - h(x_k + \widehat{\delta x}_{k|k-1})), \qquad (4)$$
$$P_{k|k} = (I - K_k H_k)P_{k|k-1},$$

where $h(\cdot)$ is the observation function of the sensor, H is its the Jacobian and I is the identity matrix. In the ESKF, following the update step, the corrected error state, $\widehat{\delta x}_{k|k}$ is injected into the nominal state, and the error state estimate $\widehat{\delta x}_{k|k}$ is reset to zero:

$$x_{k+1} = x_k \oplus \widehat{\delta x}_{k|k}^-, \qquad (5)$$
$$\widehat{\delta x}_{k|k} = [0].$$

where $\oplus$ denotes the composition operation. Due to this step, the error state estimate $\widehat{\delta x}_{k-1|k-1}$ in the prediction step is always zero, and Eq. (3a) does not need to be computed [14].

III. ESKF FORMULATION FOR NAVIGATION

To formulate the ESKF for navigation, we use the approach adopted by Sola [22], representing attitudes with unit Hamilton quaternions. We also use the local tangent plane North-East-Down (NED) fixed to the Earth since we focus on local navigation for Urban Air Mobility. For the prediction step and nominal state integration, we use a kinematic model to be vehicle-independent, and stochastic models for the INS sensor and GNSS bias.

A. INS model

From the inertial navigation system, we use acceleration and angular velocities as inputs to the kinematic model. Their dynamics are modeled with Gaussian and Brownian noises, as follows:

$$a_m = R_t^T(a_t - g_t) + a_b + a_n, \qquad (6)$$
$$\dot{a}_b = a_w.$$

$$\omega_m = \omega_{body} + \omega_b + \omega_n, \qquad (7)$$
$$\dot{\omega}_b = \omega_w$$

where a_m is the measured acceleration, R_t is the true attitude matrix, a_t is the true acceleration in NED, g_t is gravity in NED, a_b accelerometer bias, $a_n \sim \mathcal{N}(0, \sigma_{a_n}^2)$, $a_w \sim \mathcal{N}(0, \sigma_{a_w}^2)$, ω_m is the measured angular velocity, ω_{body} is the true angular velocity in the body frame, ω_b is the angular velocity bias, $\omega_n \sim \mathcal{N}(0, \sigma_{\omega_n}^2)$, and $\omega_w \sim \mathcal{N}(0, \sigma_{\omega_w}^2)$.

B. GNSS bias model

The GNSS receiver clock bias is modeled as a second-order system

$$\dot{b} = d + v_b$$
$$\dot{d} = v_d \qquad (8)$$

where b is the receiver clock bias, d is the clock drift, $v_b \sim \mathcal{N}(0, \sigma_{v_b}^2)$, and $v_d \sim \mathcal{N}(0, \sigma_{v_d}^2)$

C. Nominal State and Prediction Step

The nominal states in discrete time are derived from the kinematics of a rigid body:

$$p_{k+1} = p_k + v_k\Delta t + \tfrac{1}{2}(R_{q2R}\{q_k\}(a_{m,k} - a_{b,k}))\Delta t^2,$$
$$v_{k+1} = v_k + (R_{q2R}\{q_k\}(a_{m,k} - a_{b,k}) + g_k)\Delta t,$$
$$q_{k+1} = q_k \otimes q_{v2q}\{(\omega_{m,k} - \omega_{b,k})\Delta t\},$$
$$a_{b,k+1} = a_{b,k},$$
$$\omega_{b,k+1} = \omega_{b,k},$$
$$b_{k+1} = b_k + d_k\Delta t,$$
$$d_{k+1} = d_k, \qquad (9)$$

where p is the position in NED, v is the velocity in NED, q is the attitude quaternion, $R_{q2R}\{\cdot\}$ is the attitude matrix calculated from the attitude quaternion, $q_{v2q}\{\cdot\}$ is the quaternion calculated from the rotation vector, and $\otimes$ denotes the quaternion product. The nominal states, error states, system inputs, and disturbances are respectively

$$x = \begin{bmatrix} p & v & q & a_b & \omega_b & g \end{bmatrix}',$$
$$\delta x = \begin{bmatrix} \delta p & \delta v & \delta\theta & \delta a_b & \delta\omega_b & \delta g \end{bmatrix}',$$
$$u_m = \begin{bmatrix} a_m & \omega_w \end{bmatrix}', \qquad (10)$$
$$i = \begin{bmatrix} v_i & \theta_i & a_i & \omega_i & v_b & v_i \end{bmatrix}'$$

The Jacobian of error states is

$$F_{\delta x} = \begin{bmatrix}
I_3 & I_3\Delta t & 0_3 & 0_3 & 0_3 & 0_3 & 0_{3\times2} \\
0_3 & I_3 & A & C & 0_3 & I_3\Delta t & 0_{3\times2} \\
0_3 & 0_3 & B & 0_3 & -I_3\Delta t & 0_3 & 0_{3\times2} \\
0_3 & 0_3 & 0_3 & I_3 & 0_3 & 0_3 & 0_{3\times2} \\
0_3 & 0_3 & 0_3 & 0_3 & I_3 & 0_3 & 0_{3\times2} \\
0_3 & 0_3 & 0_3 & 0_3 & 0_3 & I_3 & 0_{3\times2} \\
0_{2\times3} & 0_{2\times3} & 0_{2\times3} & 0_{2\times3} & 0_{2\times3} & 0_{2\times3} & \begin{bmatrix} 1 & \Delta t \\ 0 & 1 \end{bmatrix}
\end{bmatrix},$$

$$A = -R_{q2R}\{q_k\}[a_m - a_b]_\times\Delta t,$$
$$B = R_{v2R}\{(\omega_m - \omega_b)\Delta t\},$$
$$C = -R_{q2R}\{q_k\}\Delta t. \qquad (11)$$

where R_{v2R} is the rotation matrix from the error rotation vector. The model process covariance is given by

$$F_i = \begin{bmatrix}
0_3 & 0_3 & 0_3 & 0_3 & 0_{3\times2} \\
I_3 & 0_3 & 0_3 & 0_3 & 0_{3\times2} \\
0_3 & I_3 & 0_3 & 0_3 & 0_{3\times2} \\
0_3 & 0_3 & I_3 & 0_3 & 0_{3\times2} \\
0_3 & 0_3 & 0_3 & I_3 & 0_{3\times2} \\
0_{2\times3} & 0_{2\times3} & 0_{2\times3} & 0_{2\times3} & I_2
\end{bmatrix}, \qquad (12)$$

$$Q_i = \begin{bmatrix}
\sigma_v^2\Delta t^2 I_3 & 0_3 & 0_3 & 0_3 & 0_{3\times2} \\
0_3 & \sigma_\theta^2\Delta t^2 I_3 & 0_3 & 0_3 & 0_{3\times2} \\
0_3 & 0_3 & \sigma_a^2\Delta t^2 I_3 & 0_3 & 0_{3\times2} \\
0_3 & 0_3 & 0_3 & \sigma_\omega^2\Delta t^2 I_{3x2} & 0_3 \\
0_3 & 0_3 & 0_3 & 0_3 & Q_c
\end{bmatrix}, \qquad (13)$$

$$Q_c = \sigma_{v_b}^2 \begin{bmatrix} \Delta t & 0 \\ 0 & 0 \end{bmatrix} + \sigma_{v_d}^2 \begin{bmatrix} \tfrac{1}{3}\Delta t^3 & \tfrac{1}{2}\Delta t^2 \\ \tfrac{1}{2}\Delta t^2 & \Delta t \end{bmatrix}. \qquad (14)$$

IV. SENSOR MODELS AND UPDATE STEP

In the update step, we use a GNSS sensor modeled in three different ways for comparison and a camera to detect Fiducial markers.

A. GNSS linear model

We model the GNSS as a linear sensor to evaluate how the filter performs with an ideal sensor. The GNSS is able to directly measure the positions and velocities of the aircraft with

$$h_{GNSS}(\boldsymbol{x}_k) = \begin{bmatrix} I_6 & 0_{6 \times 10} \end{bmatrix} \boldsymbol{x}_k, \tag{15}$$

and its Jacobian is

$$H_{GNSS} = \begin{bmatrix} I_6 & 0_{6 \times 10} \end{bmatrix} X_{\delta x}, \tag{16}$$

$$X_{\delta x} = \begin{bmatrix} I_6 & 0_{6 \times 4} & 0_{6 \times 9} \\ 0_{4 \times 6} & Q_{\delta \theta} & 0_{4 \times 9} \\ 0_{9 \times 6} & 0_{9 \times 4} & I_9 \end{bmatrix}, Q_{\delta x} = \frac{1}{2} \begin{bmatrix} -q_x & -q_y & -q_z \\ q_w & -q_z & q_y \\ q_z & q_w & -q_x \\ -q_y & q_x & q_w \end{bmatrix}. \tag{17}$$

The covariance matrix is

$$V_{GNSS} = diag(n_{\text{dop}}^2 \sigma_r^2, \quad e_{\text{dop}}^2 \sigma_r^2, \quad v_{\text{dop}}^2 \sigma_r^2, \quad \cdots \\ \cdots \quad n_{\text{dop}}^2 \sigma_v^2, \quad e_{\text{dop}}^2 \sigma_v^2, \quad v_{\text{dop}}^2 \sigma_v^2), \tag{18}$$

where n_{dop}, e_{dop} and v_{dop} are the dilution of precision for north, east, and down, σ_r is the user equivalent range error and σ_v is the range rate error. With the linear model, we use nominal and prediction equations without the GNSS bias states resulting in 16 states instead of 18.

B. GNSS pseudorange model

The pseudorange model uses a GPS constellation model with Keplerian orbits according to the GPS SPS performance standard [23] and the interface control document IS-GPS-200M [24]. The observation function of the pseudoranges is

$$h_\rho(\boldsymbol{x}_k) = \begin{bmatrix} h_{\rho,1} & \cdots & h_{\rho,n} \end{bmatrix}^T, \\ h_{\rho,j} = r_j + cb_k, \\ r_j = \sqrt{\|\Delta \boldsymbol{p}_{k,j}\|_2}, \\ \Delta \boldsymbol{p}_{k,j} = \boldsymbol{p}_k^e - \boldsymbol{p}_{k,j}. \tag{19}$$

where n is the number of visible satellites considering a mask angle m_A; $\boldsymbol{p}_k^e = \begin{bmatrix} x_k^e & y_k^e & z_k^e \end{bmatrix}^T$ are the aircraft coordinates in the ECEF frame, $\boldsymbol{p}_{k,j}$ are the satellite j ECEF coordinates, and c is the speed of light constant. The Jacobian is

$$H_\rho = \frac{\partial h_{\rho,j}}{\partial x_\rho} \frac{\partial x_\rho}{\partial x} X_{\delta x}, \ x_\rho = \begin{bmatrix} x_k^e & y_k^e & z_k^e & b \end{bmatrix}^T \\ \frac{\partial h_{\rho,j}}{\partial x_p} = \begin{bmatrix} \frac{x_k^e}{r_j} & \frac{y_k^e}{r_j} & \frac{z_k^e}{r_j} & c \end{bmatrix} \\ \frac{\partial x_p}{\partial x} = \begin{bmatrix} R_{te} & 0_{3 \times 13} & 0_{3 \times 1} & 0_{3 \times 1} \\ 0_{1 \times 3} & 0_{1 \times 13} & 1 & 0 \end{bmatrix} \\ R_{te} = \begin{bmatrix} -sin(\phi_0)cos(\lambda_0) & -sin(\lambda_0) & -cos(\phi)cos(\lambda) \\ -sin(\phi_0)sin(\lambda_0) & cos(\lambda_0) & -cos(\phi_0)sin(\lambda_0) \\ cos(\phi_0) & 0 & -sin(\phi_0) \end{bmatrix} \tag{20}$$

where ϕ_0 is the reference latitude, and λ_0 is the reference longitude for the NED frame.

The noise covariance matrix is

$$V_p = I_n \sigma_p^2 \tag{21}$$

C. GNSS pseudorange and pseudorange rate model

In this model, in addition to the pseudorange, we also add the pseudorange rate measurements from the receiver. The total observation function becomes

$$h_{\rho\dot{\rho}}(\boldsymbol{x}_k) = \begin{bmatrix} h_\rho \\ h_{\dot\rho} \end{bmatrix}, h_{\dot\rho} = \begin{bmatrix} h_{\dot\rho,1} & \cdots & h_{\dot\rho,n} \end{bmatrix}^T \\ \Delta \boldsymbol{v}_{k,j} = \boldsymbol{v}_k^e - \boldsymbol{v}_{k,j} \\ h_{\dot\rho,j} = \frac{\Delta \boldsymbol{v}_{k,j} \cdot \Delta \boldsymbol{x}_{k,j}}{r_j} \tag{22}$$

where $\boldsymbol{v}_k^e = \begin{bmatrix} v_{x,k}^e & v_{y,k}^e & v_{z,k}^e \end{bmatrix}^T$ are the aircraft velocities in ECEF frame and $\boldsymbol{v}_{k,j}$ are the satellite j velocities in ECEF frame. Therefore the Jacobian is

$$H_{\rho,\dot\rho} = \begin{bmatrix} H_\rho \\ H_{\dot\rho} \end{bmatrix}, \ H_{\dot\rho} = \frac{\partial h_{\dot\rho,j}}{\partial x_{\dot\rho}} \frac{\partial x_{\dot\rho}}{\partial x} X_{\delta x}, \\ \boldsymbol{x}_{\dot\rho} = \begin{bmatrix} x_k^e & y_k^e & z_k^e & v_{x,k}^e & v_{y,k}^e & v_{z,k}^e \end{bmatrix}^T, \\ \frac{\partial h_{\dot\rho,j}}{\partial x_\rho} = \begin{bmatrix} \frac{\Delta v_{k,l}}{r_j} & \frac{\Delta P_{k,l}}{r_j} \end{bmatrix}, \\ \frac{\partial x_{\dot p}}{\partial x} = \begin{bmatrix} R_{te} & 0_3 & 0_{3 \times 12} \\ 0_3 & R_{te} & 0_{3 \times 12} \end{bmatrix}, \tag{23}$$

with noise covariance matrix

$$V_{p\dot{p}} = \begin{bmatrix} I_n \sigma_p^2 & 0_n \\ 0_n & I_n \sigma_{\dot p}^2 \end{bmatrix}. \tag{24}$$

D. Camera and Fiducial Marker

The fiducial marker used in this work is the April Tag [16] and is detected by a camera pointing down from the aircraft. For our camera model, we use a pinhole camera with no distortion. The pose measurement with the April Tag library uses the tag size and the camera intrinsic parameters f_x, f_y, c_x, and c_y which are the focal length and optical center in x and y.

The April Tag pose detection can measure the position and orientation of the tags with respect to the camera. We transform these detections to aircraft pose measurements with homogeneous transformations, starting from the tag pose in the NED frame to the camera, then from the camera to the aircraft body frame. After the transformation, we have an observation function given by

$$h_m = \begin{bmatrix} h_p \\ h_q \end{bmatrix}, h_p = \begin{bmatrix} x_k & y_k & z_k \end{bmatrix}^T, \ h_q = \text{rv}(\boldsymbol{q_k}), \tag{25}$$

where $\text{rv}(\cdot)$ is the quaternion to rotation vector conversion. Although the orientation is observed in the quaternion space, we model the Gaussian noises in the rotation vector space such that the measurement equation becomes

$$z_{k,m} = \begin{bmatrix} z_{k,p} \\ z_{k,q} \end{bmatrix} = \begin{bmatrix} h_p(\boldsymbol{x_k}) + \boldsymbol{v_{mp}} \\ \text{rv}(\boldsymbol{q_k} \otimes q_{v2q}\{\boldsymbol{v_{mq}}\}) \end{bmatrix}, \tag{26}$$

which models the marker detection of the April Tag in the image. Due to the quaternion, the innovation is calculated with the quaternion difference:

$$\tilde{y}_k = \begin{bmatrix} z_p - h_p \\ \text{rv}(\text{conj}(q_{v2q}\{h_p\})(q_{v2q}\{z_{k,q}\})) \end{bmatrix} \tag{27}$$

Thence the Jacobian of this measurement is

$$H_m = \begin{bmatrix} I_3 & 0_3 & 0_3 & 0_{3 \times 12} \\ 0_3 & 0_3 & I_3 & 0_{3 \times 12} \end{bmatrix}. \tag{28}$$

The noise covariance matrix of the measurements is

$$V_m = \begin{bmatrix} I_3 \sigma_{v_{mp}}^2 & 0_3 \\ 0_3 & I_3 \sigma_{v_{mq}}^2 \end{bmatrix} \quad . \tag{29}$$

V. SIMULATION RESULTS

In this section, we evaluate the ESKF with different sensor models. To analyze filter consistency, we use the average normalized estimation error squared (ANEES) [6] over 50 Monte Carlo Simulations. The sensor parameters for the INS are: frequency = 100 Hz, $\sigma_{a_n} = 5.3 \cdot 10^{-3}$ m/s^2, $\sigma_{a_w} = 3.6 \cdot 10^{-2}$ m/s^2, $\sigma_{\omega_n} = 10^{-2}$ rad/s, $\sigma_{\omega_w} = 10^{-4}$ rad/s^2. For the GNSS: frequency = 5 Hz, $\sigma_r = 10$ m, $\sigma_r = 0.02$ m/s, $\sigma_{v_b}^2 = 110^{-19}$ s, $\sigma_{v_b}^2 = 2\pi^2 2 \cdot 10^{-20}$, $\phi_0 = -23.217936°$, $\lambda_0 = -45.891734°$, $m_A = 5°$. For the Fiducial Marker pose estimate: $\sigma_{v_{mpxy}} = 2$ m, $\sigma_{v_{mpz}} = 2$ m, $\sigma_{v_{mq}} = 0.15$ rad, for the camera: frame rate = 20 fps, $f_x = 1109$ px, $f_y = 1109$ px, $c_x = 640$ px, $c_y = 360$ px, image size = 720×1280 px. The April Tag family "36h11" is used with size = 0.8 m.
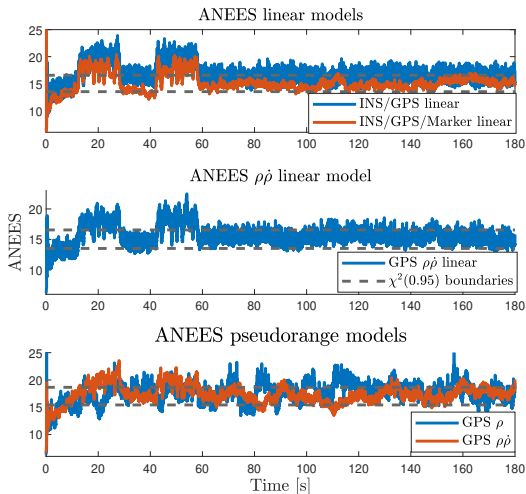
Fig. 1.   Average Normalized Estimation Error Squared for the navigation ESKF models.

Figure 1 shows the ANEES analysis results. The GNSS linear model and INS/GNSS/Marker linear model simulations both use Gaussian noises to generate the sensor measurements and are consistent with the $\chi^2(0.95)$ test after 60 s, when our aircraft flies with constant velocity, staying 96.33% and 98.38% within the boundaries respectively. With the INS/GNSS $\rho\dot{\rho}$ filter we use the pseudorange measurements to calculate NED coordinates and velocities and update the filter with the linear model. The ANEES metric for this filter is also consistent at 96.98%; The INS/GNSS ρ filter uses only the pseudorange updates, and due to the larger errors, fails the consistency test but stays 84.92% within the boundaries. The INS/GNSS $\rho\dot{\rho}$ filter uses pseudorange and pseudorange rate updates, staying 91.41% within the boundaries.

The RMSE in Table I shows that the pseudorange and pseudorange rate filter has the best accuracy for position, velocity, and attitudes when the GNSS sensor model the satellite orbits. The INS/GNSS/Marker ON/OFF simulates the first half of the trajectory with only the marker and the second half with only GPS, showing that the Marker can substitute the GPS when it is not available.

To validate the filter in a more realistic scenario we use the Unreal Engine environment integrated with Matlab, where we generate synthetic images for the aircraft ground truth in an urban environment. The images are used for marker detection and aircraft pose estimate with the camera when markers are in the field of view. The GNSS model used generates the pseudorange measurements with clock bias and pseudorange rate measurements.

Figure 2 shows the camera view in the initial position with the marker detection. We placed the marker at the initial position and the aircraft performed an 'L' shaped motion at an altitude of 15 m. From 0 s to 60 s it moves 28 m North, returns to origin, moves 28 m East, and returns to origin, with attitude varying accordingly to rotary-wing aircraft, then up to 180 s it moves Northeast with constant velocity and zero attitude.
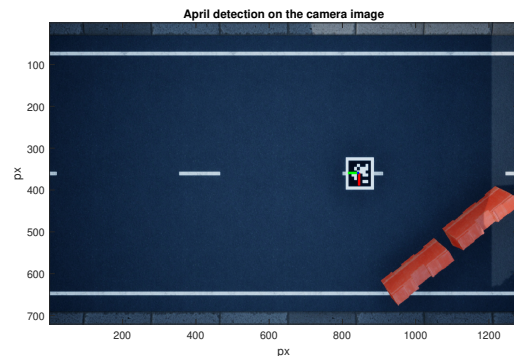
Fig. 2.   April Tag detection in the camera image at the initial position.

The results for the pseudorange and pseudorange filter with the Unreal simulation show that the filter can correctly estimate the aircraft position, velocity, and attitude in Fig. 3, and all the sensor biases in Fig. 4. Note that, after 60 s, since the aircraft moves with constant velocity and attitude, the yaw loses observability.

The RMSE results in Table I show that the marker measurements greatly improve filter accuracy, even though they are only available for a few sections of the route.
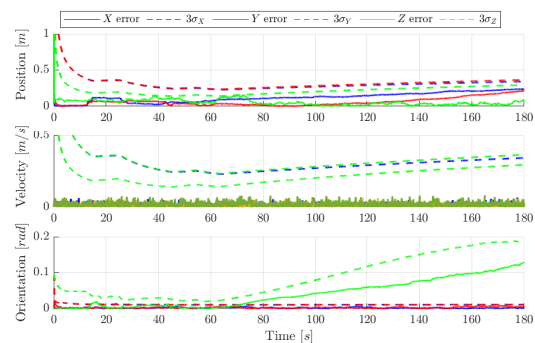
Fig. 3.   Unreal Simulation: Position Error, Velocity Error, Orientation Error.

TABLE I

ROOT MEAN SQUARE ERROR (RMSE) FOR THE ESKF MODELS

Filter	iter	x	y	z	v_x	v_y	v_z	θ_x	θ_y	θ_z
INS/GPS linear	50	0.5086	0.4999	1.2706	0.0103	0.0103	0.0082	0.0069	0.0075	0.0341
INS/GPS/Marker linear	50	0.1778	0.1775	0.3058	0.0101	0.0100	0.0082	0.0038	0.0040	0.0129
INS/GPS $p\dot{\rho}$ linear	50	0.6340	0.6112	1.3658	0.0114	0.0119	0.0094	0.0070	0.0078	0.0340
INS/GPS ρ	50	0.8230	0.8802	1.6383	0.3913	0.3893	0.1172	0.0108	0.0111	0.0278
INS/GPS $\rho\dot{\rho}$	50	0.4448	0.3727	1.5157	0.0090	0.0096	0.0094	0.0068	0.0076	0.0327
INS/GPS/Marker ON/OFF	50	0.5464	0.5600	1.1363	0.1409	0.1389	0.0152	0.0064	0.0072	0.0176
INS/GPS/Marker Unreal	1	0.0823	0.1616	0.4109	0.0075	0.0092	0.0092	0.0030	0.0029	0.0191
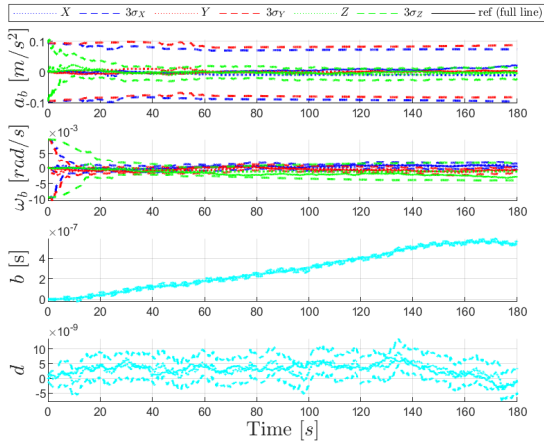
Fig. 4. Unreal Simulation: Accelerometer Bias, Gyrometer Bias, GNSS Clock Bias.

VI. CONCLUSIONS

In this paper we formulate the ESKF for navigation to fuse data from INS, GNSS modeled with pseudoranges and Fiducial Marker pose measurements detected by a camera. We evaluate filter consistency and RMSE. The results are validated in simulation with synthetic images and pseudorange measurements from simulated satellite orbits. The simulation results show that the Fiducial Marker can both increase the navigation accuracy and substitute the GNSS when the latter is not available.

AKNOWLEDGEMENTS

REFERENCES

[1] Stouffer, Virginia L., et al. "Reliable, secure, and scalable communications, navigation, and surveillance (CNS) options for urban air mobility (UAM)." *NASA Technical Reports Server* (2020).

[2] Ertürk, M. Cenk, et al. "Requirements and technologies towards uam: Communication, navigation, and surveillance." 2020 Integrated Communications Navigation and Surveillance Conference (ICNS). *IEEE*, 2020.

[3] Mueller, Eric R., Parmial H. Kopardekar, and Kenneth H. Goodrich. "Enabling airspace integration for high-density on-demand mobility operations." 17th AIAA Aviation Technology, Integration, and Operations Conference. 2017.

[4] Straubinger, Anna, et al. "An overview of current research and developments in urban air mobility–Setting the scene for UAM introduction." Journal of Air Transport Management 87 (2020): 101852.

[5] Farrell, Jay. Aided navigation: GPS with high rate sensors. McGraw-Hill, Inc., 2008.

[6] Bar-Shalom, Yaakov, X. Rong Li, and Thiagalingam Kirubarajan. Estimation with applications to tracking and navigation: theory algorithms and software. John Wiley & Sons, 2001.

[7] Grewal, Mohinder S., Angus P. Andrews, and Chris G. Bartone. Global navigation satellite systems, inertial navigation, and integration. John Wiley & Sons, 2020.

[8] Grewal, Mohinder S., and Angus P. Andrews. "Applications of Kalman filtering in aerospace 1960 to the present [historical perspectives]." IEEE Control Systems Magazine 30.3 (2010): 69-78.

[9] St-Pierre, Mathieu, and Denis Gingras. "Comparison between the unscented Kalman filter and the extended Kalman filter for the position estimation module of an integrated navigation information system." IEEE Intelligent Vehicles Symposium, 2004. IEEE, 2004.

[10] Crassidis, John L. "Sigma-point Kalman filtering for integrated GPS and inertial navigation." IEEE Transactions on Aerospace and Electronic Systems 42.2 (2006): 750-756.

[11] Van Der Merwe, Rudolph, Eric Wan, and Simon Julier. "Sigma-point Kalman filters for nonlinear estimation and sensor-fusion: Applications to integrated navigation." Aiaa guidance, navigation, and control conference and exhibit. 2004.

[12] Gustafsson, Fredrik, et al. "Particle filters for positioning, navigation, and tracking." IEEE Transactions on signal processing 50.2 (2002): 425-437.

[13] Maybeck, P. S. S. M. "Stochastic models." Estimation and Control 1, Academics Press (1979).

[14] Madyastha, Venkatesh, et al. "Extended Kalman filter vs. error state Kalman filter for aircraft attitude estimation." AIAA Guidance, Navigation, and Control Conference. 2011.

[15] Roumeliotis, Stergios I., Gaurav S. Sukhatme, and George A. Bekey. "Circumventing dynamic modeling: Evaluation of the error-state kalman filter applied to mobile robot localization." Proceedings 1999 IEEE International Conference on Robotics and Automation (Cat. No. 99CH36288C). Vol. 2. IEEE, 1999.

[16] Wang, John, and Edwin Olson. "AprilTag 2: Efficient and robust fiducial detection." 2016 IEEE/RSJ International Conference on Intelligent Robots and Systems (IROS). IEEE, 2016.

[17] Garrido-Jurado, Sergio, et al. "Automatic generation and detection of highly reliable fiducial markers under occlusion." Pattern Recognition 47.6 (2014): 2280-2292.

[18] Kato, Hirokazu, and Mark Billinghurst. "Marker tracking and hmd calibration for a video-based augmented reality conferencing system." Proceedings 2nd IEEE and ACM International Workshop on Augmented Reality (IWAR'99). IEEE, 1999.

[19] Fiala, Mark. "Designing highly reliable fiducial markers." IEEE Transactions on Pattern analysis and machine intelligence 32.7 (2009): 1317-1324.

[20] Khazetdinov, Artur, et al. "Embedded ArUco: a novel approach for high precision UAV landing." 2021 International Siberian Conference on Control and Communications (SIBCON). IEEE, 2021.

[21] Qiu, Ziyi, et al. "A Global ArUco-Based Lidar Navigation System for UAV Navigation in GNSS-Denied Environments." Aerospace 9.8 (2022): 456.

[22] Sola, Joan. "Quaternion kinematics for the error-state Kalman filter." arXiv preprint arXiv:1711.02508 (2017).

[23] United States. Dept. of Defense "Global Positioning System Standard Positioning Service Performance Standard", GPS.gov , 2008, https://www.gps.gov/technical/ps/2008-SPS-performance-standard.pdf

[24] Flores, Anthony "GPS Interface Specification IS-GPS-200, Revision M - May 2021", GPS.gov, 2021 ,https://www.gps.gov/technical/icwg/IS-GPS-200M.pdf